Slow geodynamics and fast morphotectonics in the far east Tethys

L. Husson, N. Riel, S. Aribowo, C. Authemayou, G. de Gelder, B. J. P. Kaus, C. Mallard, D. H. Natawidjaja, Kevin Pedoja, A. C. Sarr

Geochemistry, Geophysics, Geosystems®

AGU ADVANCING EARTH AND SPACE SCIENCE

RESEARCH ARTICLE
10.1029/2021GC010167

Special Section:
Tethyan dynamics: from rifting to collision

Slow Geodynamics and Fast Morphotectonics in the Far East Tethys

L. Husson[1], N. Riel[2], S. Aribowo[1,3], C. Authemayou[4], G. de Gelder[1], B. J. P. Kaus[2], C. Mallard[5], D. H. Natawidjaja[3], K. Pedoja[6], and A. C. Sarr[7]

[1]Institut des Sciences de la Terre, CNRS, Université Grenoble Alpes, Grenoble, France, [2]Institute of Geosciences, Johannes Gutenberg University Mainz, Mainz, Germany, [3]Research Center for Geotechnology, Indonesian Institute of Sciences (LIPI), Bandung, Indonesia, [4]LGO, IUEM, CNRS, Université de Brest, Plouzané, France, [5]School of Geosciences, University of Sydney, Sydney, NSW, Australia, [6]M2C, Université de Caen, Caen, France, [7]CEREGE, Aix-Marseille Université, Aix-en-Provence, France

Abstract How can the sluggish, long-wavelength mantle convection be expressed by so many time and space scales of morphotectonic activity? To investigate these relationships, we explore the Java-Banda subduction zone, where geodynamic records cluster. In the far-East Tethys, the exceptionally arcuate Banda subduction zone circumscribes the deepest oceanic basin on Earth, seismotectonic activity slices the upper plate more efficiently than anywhere else, and uncommonly vast expanses of continents are flooded in Sundaland and Northern Australia. By comparing numerical simulations of subduction dynamics to a set of independent observations, we reveal the many facets of tectonic and physiographic changes that the sole docking of the Australian continent onto the subduction zone triggered. While mantle flow remains slow and long-wavelength at depth, intense tectonic activity, and dynamic uplift and subsidence profoundly rework the physiography at many spatial scales. These results demonstrate that a modest disruption in the slow geodynamic tempo may trigger manifold morphotectonic disturbances.

Key Points:

- Fast and short-lived disruption in surface morphotectonics occur at all spatial scales during transient phases of mantle flow
- Uncommon SE Asia seismotectonic activity, dynamic topography, and vertical land motion all triggered by the transience of mantle flow
- Depiction of the intricate relationships between mantle dynamics and surface morphotectonics

Supporting Information:

Supporting Information may be found in the online version of this article.

Correspondence to:

L. Husson,
laurent.husson@univ-grenoble-alpes.fr

Citation:

Husson, L., Riel, N., Aribowo, S., Authemayou, C., de Gelder, G., Kaus, B. J. P., et al. (2022). Slow geodynamics and fast morphotectonics in the far East Tethys. *Geochemistry, Geophysics, Geosystems*, *23*, e2021GC010167. https://doi.org/10.1029/2021GC010167

Received 14 SEP 2021
Accepted 9 JAN 2022

1. Introduction

"Plate tectonics is the surface expression of mantle convection" is commonplace, but ever since Holmes (1931) seeded this concept, geological observations seem to defy this convenient rationalization of plate tectonics and mantle flow. In the vicinity of plate boundaries, the morphotectonic evolution of active plate boundaries occurs at length and timescales that are seemingly at odds with the long-wavelength and slow pace of mantle convection. Therefore, the links between mantle convection and surface tectonics remain challenging to disentangle (Davies et al., 2019; Jolivet et al., 2018; Mallard et al., 2016). At the far East end of the Tethys subduction zone, the Java-Banda subduction zone displays a unique collection of morphotectonic events that occur at various time and space scales that epitomizes this paradox. Whether these events are caused by the congestion of profuse subductions and collisions is plausible, but only few studies attempt to comprehensively analyze this possibility (Hall, 2017).

Perhaps the most puzzling observation is the pervasive flooding of vast continental units: Sahul in North Australia, and Sundaland in West Indonesia, are the largest expanses of continents to lie below sea level on Earth and are currently subsiding (Sarr, Husson, et al., 2019; Solihuddin et al., 2015). Another salient characteristic of the region is the Weber Deep, which lies at depths of more than 7 km, making it the deepest region on Earth, besides oceanic trenches. After the Banda slab rolled back to the eastern dead-end of the Banda embayment (Milsom, 2001; Spakman & Hall, 2010), the Banda basin is now nested and circumscribed by the extremely tight, horseshoed Banda arc (Figure 1). Intense seismotectonic activity is yet another remarkable facet of the region, the back-arc domain being more commonly hit by devastating earthquakes (like the Flores, Alor, and Lombok earthquakes, Figure 1) than in any other subduction zone. Each of the above geodynamic oddities has been scrutinized in one way or another but seldom as components, or surface expressions, of a unique, coupled mantle-lithosphere system. Here instead, we hypothesize that a single event, the inception of the Australian continent into the Java-Banda trench, is in fact sufficient to explain the development of multiple morphotectonic events that altogether profoundly and swiftly remodeled the physiographic layout of the entire region.

The Indian-Australian oceanic lithosphere subducted underneath SE Asia during the Cenozoic closure of the Neo-Tethys. This regime prevailed until the inception of the continent in the subduction zone in the East during

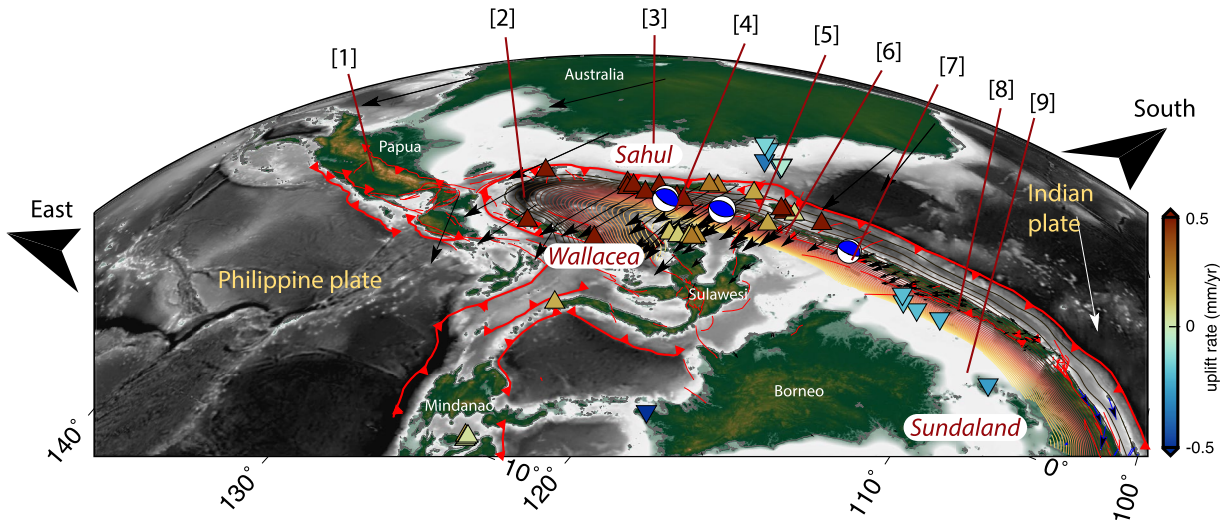

Figure 1. Morphotectonic map of SE Asia, southeastward view. The map depicts tectonic structures (faults: red curves; subduction trenches: red bold curves), envelope of the subducting plate (depth isocontours 20 m), uplift and subsidence rates (triangles, see Section 2), selected focal mechanisms (Mw > 6.5, Wetar-Flores back-arc thrust) and geodetic velocities (Koulali et al., 2016). Geodynamic extremes include [1] Papua orogen, [2] Weber superdeep basin, [3] subsiding Sahul platform, [4] Timor slab hole, [5] Savu Sea, [6] Flores back-arc thrust, [7] Lombok 2018, Alor 2004, Flores 1992 earthquakes, [8] Java back-arc thrusts (Baribis and Kendeng belts), and [9] subsiding Sunda shelf.

the Miocene (Hall, 2017), while oceanic subduction continued to the West. At the onset of collision of the Australian continent with the island arc, the lithospheres on both sides of the subduction zone were paved with alternating oceanic and continental lithospheres. The subducting plate was composed of the Indian oceanic lithosphere in the West and the Australian continent in the East, respectively converging with continental Sundaland and a mostly oceanic domain. At present, the tessellated tectonic layout mostly remains, except that the northeastern quadrant has been intensively reworked to form the complex assemblage of continental and oceanic units of Wallacea (Figure 1). Here, by means of three-dimensional numerical models of mantle and lithosphere dynamics (Kaus et al., 2016) that we match to a set of surface and subsurface tectonic, physiographic, and kinematic observations, we analyze the multiple consequences of the transient regime that followed the arrival of the Australian continent into the subduction zone. We focus on the remodeling of the large-scale mantle and lithosphere dynamics and how this disruption triggered a collection of surface morphotectonic events that are commonly analyzed in isolation from one another. Besides reproducing the first-order regional features of dynamic topography and regional plate tectonics, the simulations also outline the many time and space scales of the surface responses to the sluggish dynamics of the Earth interior.

2. Materials and Methods

2.1. Numerical Model

We perform 3-D geodynamic simulations using LaMEM (Kaus et al., 2016). This finite difference staggered grid discretization code uses particle-in-cell methods to solve the energy, momentum, and mass conservation equations. The rheologies of the rocks are assumed to be visco-elasto-plastic and the total deviatoric strain rate is given by:

$$\dot{\epsilon}_{ij} = \dot{\epsilon}^{vis}_{ij} + \dot{\epsilon}^{el}_{ij} + \dot{\epsilon}^{pl}_{ij} = \frac{1}{2\eta_{eff}}\tau_{ij} + \frac{1}{2G}\frac{\partial \tau_{ij}}{\partial t} + \dot{\lambda}\frac{\partial Q}{\partial \sigma_{ij}},$$

where $\dot{\epsilon}^{vis}_{ij}$, $\dot{\epsilon}^{el}_{ij}$, and $\dot{\epsilon}^{pl}_{ij}$ are the viscous, elastic, and plastic strain rates, respectively. η_{eff} is the effective viscosity, G the elastic shear modulus, τ_{ij} the deviatoric stress tensor, t the time, $\dot{\lambda}$ is the plastic multiplier, Q the plastic flow potential and $\sigma_{ij} = -P + \tau_{ij}$ the total stress. The effective viscosity η_{eff} is given by:

$$\eta_{eff} = \frac{1}{2}A^{\frac{-1}{n}}\exp\left(\frac{E + PV}{nRT}\right)\dot{\epsilon}_{II}^{\frac{1}{n}-1},$$

Table 1
Material Parameters Used in This Study

Unit	ρ (kg m^{-3})	Rheology	A (Pa^{-n} s^{-1})	E (J mol^{-1})	n	V (m^{-3} mol^{-1})	ϕ (°)	C (MPa)
Upper mantle	3,300	Dry olivine (Hirth & Kohlstedt, 2004)	1.1×10^5	530×10^3	3.5	12×10^{-6}	20	30
Lower mantle	3,600	Dry olivine (Hirth & Kohlstedt, 2004)	1.1×10^5	530×10^3	3.5	12.6×10^{-6}	20	30
Oceanic crust	3,300	Diabase (Mackwell et al., 1998)	8	485×10^3	4.7	0	0	5
Continental crust	2,800	Quartzite (Ranalli, 1995)	6.7×10^{-6}	156×10^3	2.4	0	20	30

Note. Additional parameters, uniform across all materials are the elastic shear modulus $G = 5 \times 10^{10}$ Pa, thermal expansivity $\alpha = 3 \times 10^{-5}$ K^{-1}, heat capacity $C_p = 1{,}050$ J K^{-1}, and thermal conductivity $\kappa = 3.0$ W m^1 K^{-1}. The minimum and maximum viscosities are capped to 1×10^{19} and 1×10^{23} Pa s^1, respectively.

where A is the exponential prefactor, n the stress exponent of the dislocation creep, $\dot{\epsilon}_{II}$ is the second invariant of the viscous strain rate tensor, E, V are the activation energy and volume, respectively, P is the pressure, R is the gas constant, and T is the temperature. Plasticity is modeled using the Drucker-Prager yield criterion given by:

$$\tau_Y = \sin(\phi)P + \cos(\phi)C,$$

where τ_Y is the yield stress, ϕ the friction angle, and C the cohesion. Strain softening is taken into account by linearly reducing both the friction angle and the cohesion of the material by a factor of 100 between 10% and 60% of accumulated strain. Minimum cohesion is set to 0.01 MPa and maximum yielding stress to 900 MPa.

The modeled region is a 3-D box of dimensions $5{,}000 \times 4{,}000 \times 1{,}050$ km with a resolution of $320 \times 256 \times 128$ cells. It comprises a 50 km thick air layer, lithospheric plates (oceanic and continental) embedded in a 660 km thick upper mantle, and a 340 km thick lower mantle. Boundary conditions are no slip on the bottom, free slip on all sides and free surface with open boundary on top. The temperature is set to 20°C at the top of the model and within the air layer, and 1602°C at the bottom boundary. In order to keep the air layer at 20°C the conductivity in the air is artificially set to $\kappa = 100$ W m^{-1} K^{-1} and the heat capacity is set to $C_p = 10^6$ J K^{-1}. Initial temperature profiles within the plates are prescribed according to the half-space cooling model (Turcotte & Schubert, 1982). For continental plates (Sundaland and Australia) the thickness of the boundary layer is set to 120 km and the half-space cooling age is 110 Ma. For the lithosphere of the volcanic arc the thickness of the boundary layer is set to 100 km and the cooling age to 70 Ma. For oceanic plates, the thermal profile is set according to the half space cooling model with an 80 km thick boundary layer and the cooling age is initialized as a function of the distance to the oceanic ridge, using a spreading rate of 1.5 cm yr^{-1}. In the upper mantle and uppermost lower mantle, the initial temperature gradient is set to 0.3 K km^{-1}. Continental and oceanic crusts are respectively, 35 and 15 km thick. Material properties are given in Table 1. In practice, we performed a set of simulations that gradually incorporated complexity, starting from box models with few rheological components, toward the final model that displays a complex arrangement of oceanic and continental units as well as an island arc. In order to continuously have a weak subduction interface, the maximum strength of the oceanic crust is capped by setting up the plastic cohesion to a low value ($C = 5$ MPa). Convergence between the Indian-Australian and the Sundaland/Wallacea system is triggered by incorporating a pre-subducted segment of the oceanic plate. The subsequent geodynamic evolution is self-consistent, entirely buoyancy driven.

2.2. Bulk, Isostatic, and Dynamic Uplift Rates

Model simulations output the bulk uplift rates, accounting for both isostatic and dynamic components. At some locations, both can be significant when strain rates and mantle flow efficiently distort the surface. We disentangle the two components by approximating that the bulk uplift rate $u_{v_{\text{bulk}}}$ results from the joint effects of instantaneous crustal isostatic uplift $u_{v_{\text{iso}}}$ and dynamic uplift $u_{v_{\text{dyn}}}$:

$$u_{v_{\text{dyn}}} = u_{v_{\text{bulk}}} - u_{v_{\text{iso}}}$$

We first approximate isostatic uplift rates by computing crustal thickening rates from the divergence of the horizontal velocity at the surface ∇u_h and crustal thickness S such that

$$u_{v_{\text{iso}}} = \frac{1}{1 + \frac{\rho_m - \rho_c}{\rho^* - \rho c}} \nabla u_h S$$

where ρ_m and ρ_c are the reference densities of the mantle and crust, while $\rho*$ is the density of the loading material (air, water, and sediments).

The model output dynamic topography and dynamic uplift rates are air-compensated. Water-compensated and sediment-compensated deflections are respectively increased by a factor $\Delta\rho_a/\Delta\rho_w$ and $\Delta\rho_a/\Delta\rho_s$, where $\Delta\rho_a$, $\Delta\rho_w$, and $\Delta\rho_s$ are the density contrasts between the mantle and air, water, and sediments. Reference mantle density is set in our model to 3,300 kg m^{-3}, seawater has a density of 1,030 kg m^{-3} and we assume a density of 2,000 kg m^{-3} for recent sediments. The "maritime continent" that we model includes air-, water- and sediment-loaded topographies, and appropriate compensations need to be carefully chosen based on the geological record, when comparing model outputs to observations. In the deep Banda and Weber basins, we thus account for water compensation, while in the Sahul shelf, which is only flooded in the late stage, water- or sediment-compensations have negligible impacts. Conversely in the Sunda shelf, the platform is largely flooded and covered by layers of sediments and seawater of variable, yet limited thicknesses, indicating a combined compensation by air, water, and sediments, which does not permit to precisely *a priori* elicit one of the three compensation mechanisms. Nevertheless, we retain the intermediate situation (water-compensation) as a plausible situation between the two end-members (air- and sediment-compensation) for the time-integrated dynamic deflection. Conversely, uplift rates at present are the time derivative of the current elevation, and attest for the instantaneous compensation process. In that case, sediment-compensated subsidence below sea level most appropriately reflects the current sedimentation pattern in the Sunda shelf.

2.3. Observed Uplift and Subsidence Rates

Mean Pleistocene uplift and subsidence rates are derived from unpublished and published estimates (see Table S1 and Figure S1 in Supporting Information S1). Most rates are estimated from the geomorphology of uplifting or subsiding sequences of coral reefs. Some uplift rates are derived from the inversion of river profiles. In addition in the Sunda shelf, the shallow stratigraphy of the platform (as seen on high-resolution seismic profiles) reveals a series of incised sedimentary layers that are interpreted as fingerprints of the quickly oscillating sea level during the Quaternary. Alternating periods of marine transgressions and regressions imprint the sedimentary cover by episodes of sedimentary deposition followed by episodes of drainage. The number of these episodes indicates the number of glacial cycles during which the platform was reached by marine transgressions. This number is contingent on sea-level oscillations and bathymetry but also on subsidence rates (Sarr, Husson, et al., 2019). We use this relationship to derive new estimates of subsidence rates from a survey in North East Java (Susilohadi & Soeprapto, 2015), where 4–5 units (or 4 to 8 sub-units) have been identified. Using sea level reconstructions (Waelbroeck et al., 2002), this allows bracketing subsidence rates in the area between 0.1 and 0.25 mm/yr (Figure S2 in Supporting Information S1).

3. Results

3.1. Australian Continent Disrupts Subduction Dynamics and Mantle Flow

We explore the regional subduction dynamics and surface morphotectonics using Cartesian three-dimensional thermo-mechanical models. These simulations are "Earth-like," in the sense that the setup attempts to objectively integrate the specific geometries of the region without any a priori filtering of selected features. This choice allows us to diagnose the impact of the arrival of the Australian continent into the subduction zone on regional morphotectonics in both their temporal and spatial frameworks since the early Oligocene. More specifically, the close resemblance to real Earth facilitates the comparison of the model outcomes to our set of observations (see initial setup Figure 2). Our scenario starts prior to the collision, at a time when the Indo-Australian lithosphere subducted North of Papua during the early Oligocene. At that stage, the existence of the Banda embayment prior to collision, as well as an island arc and alternating landmasses and oceanic basins in the upper plate best account for the pre-collisional conditions (Harris, 2011). We only present our final simulation, extracted from a set of experiments on its ability to reproduce kinematic and physiographic observations (Hall, 2017; Spakman & Hall, 2010). Complete modeling approach, alternative simulations, and animations are presented in Supplementary Materials (Figures S3–S8 in Supporting Information S1).

Our simulation unravels the joint evolution of the regional physiography and mantle flow (Figure 3). The first event to disrupt the northward journey of the Australian continent is the inception of the Papuan promontory

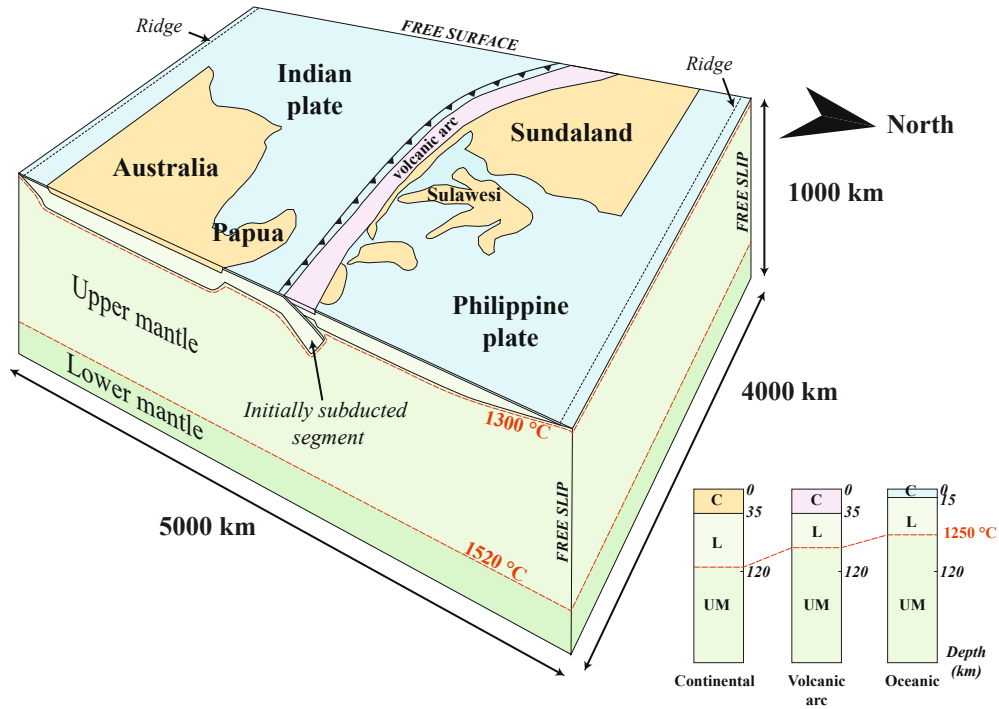

Figure 2. Initial setup of the model. The model is entirely buoyancy driven, forces arising from mantle thermal convection, from which ridge push and slab pull arise. Initial configuration is based on reconstructions (Ely & Sandiford, 2010; Hall, 2012, 2017; Hall & Spakman, 2015; Harris, 2011; Spakman and Hall., 2010). The model accounts for 3 different vertical stratifications (as depicted on the columns). The thermo-mechanical structure of the Indian and Philippine oceanic plates is set by half-space cooling away from the ridge. The shapes of continental units are defined according to their current and reconstructed geometries prior to collision. The small continental units North of Australia represent the envelope of the loosely constrained assemblage of small-size continental units prior to collision with Papua; they play a negligible role in the modeled dynamics. The volcanic arc has a more ductile behavior. See Section 2 for technical description of the thermal/mechanical aspects and Table 1 for material properties.

into the subduction zone. Until that stage, the mantle flow is essentially poloidal (in the vertical plane, mostly normal to the trench), accompanying the descent of the oceanic lithosphere in the upper mantle. Soon after, the slab breaks off and collision proceeds in Papua. In the upper mantle, a toroidal (in the horizontal plane, parallel to the surface) component of mantle flow expands during the breakoff of the slab segment underneath Papua. Mantle flow accelerates and conveys the mantle from the sub-Australian (or Indian) reservoir into the Eurasian reservoir. This revised scheme of mantle circulation facilitates rollback of the Banda slab as the trench winds around the Bird's Head, West Papua and eventually retreats and nests in the Banda embayment (Figures 3 and 4). This scenario conforms to previous kinematic reconstructions based on surface geological observations and seismic tomography (Milsom, 2001; Spakman and Hall., 2010), which depict a continuous slab that increases in convexity as it molds in the Banda embayment. At first sight, our model predictions validate the mechanics of this conceptual model. However, the situation is more complex at depth, as such trench runaway requires extreme distortions of the subducting plate. The once more linear Miocene trench running from Java to Papua is now bent enough to bear a unique slab that subducts with opposite vergences within only a few hundred kilometers along the Banda arc (Figure 1 and Figure S1 in Supporting Information S1). While breakoff underneath Papua in the North eased the retreat of the trench and the subsequent opening of the Banda back-arc basin, the situation differs in the South. After 26.8 My (forward model time, 0 My being the beginning of the simulation), the setting resembles that of present day (0 Ma actual time, Figures 3e and 3f). At that stage, not only the Australian continent has already docked onto the trench, which causes vertical tension in the subducted lithosphere (Ely & Sandiford, 2010; Royden & Husson, 2009), but eastward slab rollback also requires some longitudinal stretching of the slab, in an East-West direction, mirroring the trench elongation along the margin of North Australia by at least a factor of two (see for instance reconstructions by Spakman and Hall (2010), and Figure 4). Both geometrical constraints impose considerable distortions of the lithosphere. At the surface, this is consistent with

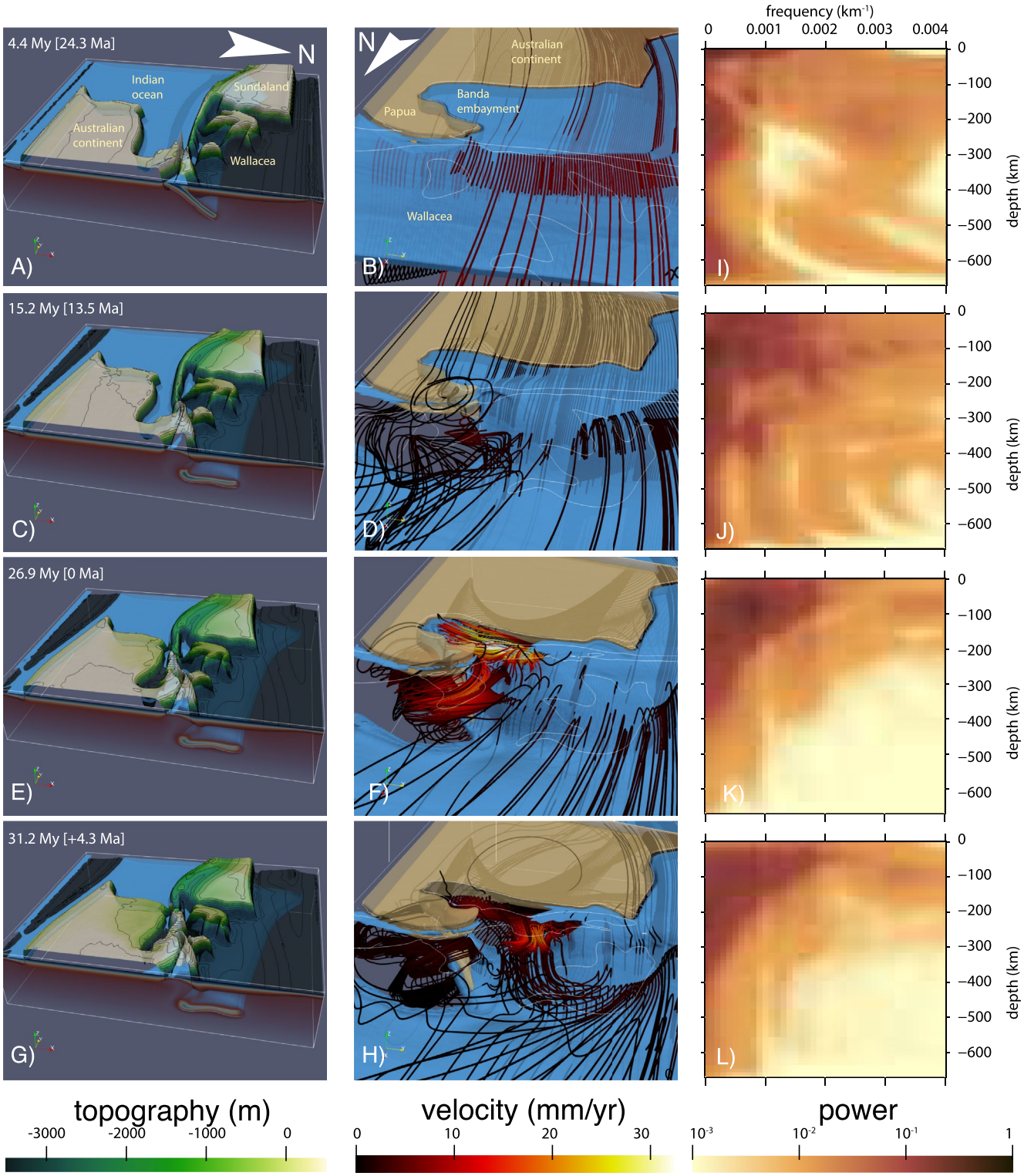

Figure 3. Model simulations of the Indo-Australian subduction zone. Time advances forward from top to bottom (model time is given in My since the beginning of the experiment, approximate equivalent Earth time is given in Ma). (a, c, e, and g) Westward views of the continental topography and Indian oceanic lithosphere (blue surface and thermal structure, eastern side view). (b, d, f, and h) Close ups of the Banda subduction zone, southward views. Indian oceanic lithosphere (blue surface) and continental units in brown (Australia) and white contours (Wallacea islands). Streamlines show mantle flow. (i, j, k, and l) Power spectrum of the strain rate in horizontal slices (normalized to the highest power). See animations in Supporting Information S1.

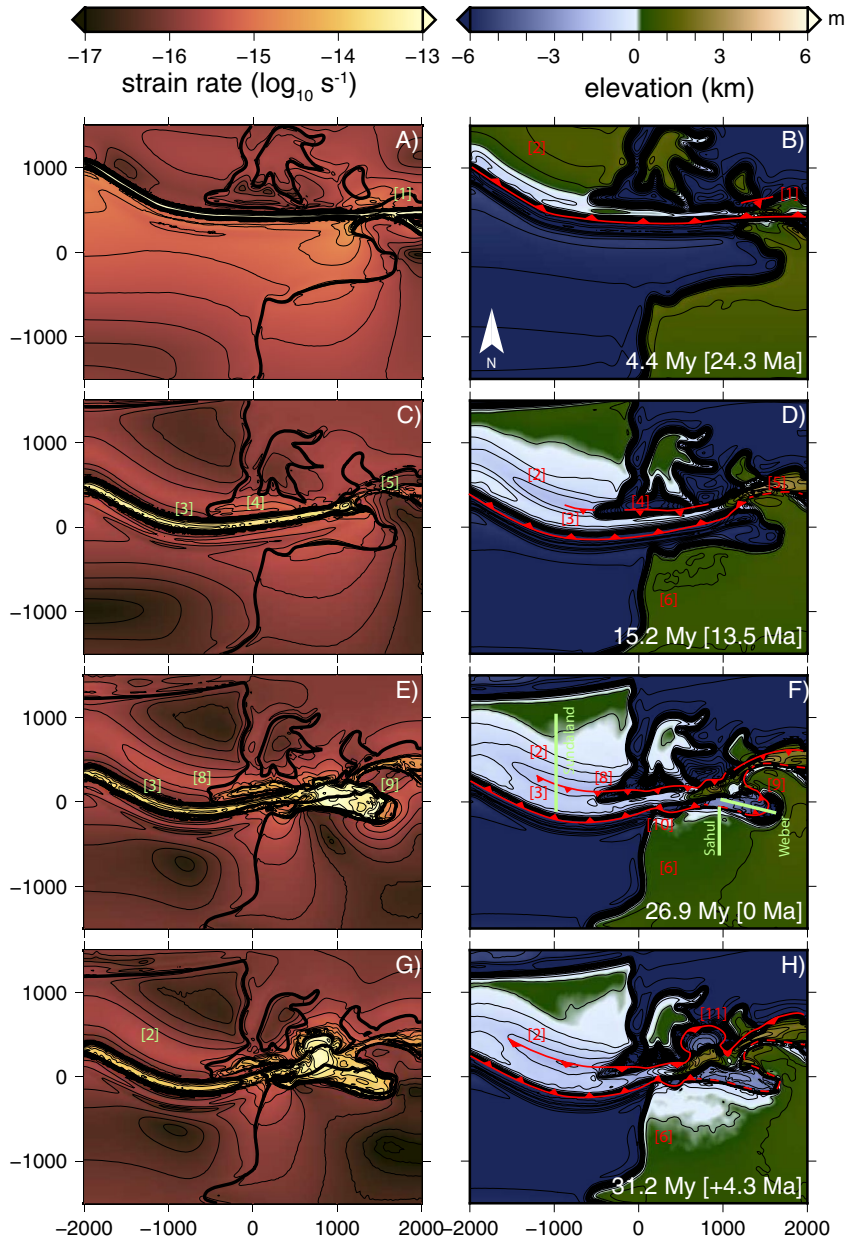

Figure 4. Modeled strain rates and topography. Time advances forward from top to bottom (model time in My, approximate equivalent Earth time in Ma). (a, c, e, and g) Surface strain rates, continental units in solid black contours. (b, d, f, and h) Elevation and interpretative tectonic framework. [1] arc-continent collision, N Papua [2] Southward tilt, Sundaland [3] incipient compression, Java [4] back-arc thrust, Wetar-Flores [5] Central range orogeny, Papua [6] Northward tilt, Australia [8] back-arc propagation to Sundaland [9] slab rollback and back-arc opening, Banda Sea [10] Savu Sea opening, and compression in Sumba [11] subduction polarity reversal.

geological observations of lithospheric delamination and with the back-arc basins that spread in the Banda Sea as the trench retreats and stretch at high strain rates (Spakman & Hall, 2010 and Figure 4). At depth, slab pull tends to neck the slab, while its eastward rollback extensively stretches it. Whether such a scenario is mechanically viable without disrupting the slab underneath Timor or Wetar is disputed. Seismic models yield contrasted results: while seismicity catalogs (Das, 2004; Ely & Sandiford, 2010) as well as some seismic tomography models (Widiyantoro & van der Hilst, 1997; Widiyantoro et al., 2011) tend to confirm slab detachment in this region, other tomographic models are less clear (Hall & Spakman, 2015) or even indicate no detachment (Harris et al., 2020; Porritt et al., 2016; Zenonos et al., 2019). Within the range of our parametric search, our simulations show little

alternative to slab tearing and breakoff. At depth, the main consequence of this event is to gradually reinforce the vigor of the toroidal cell, which in turn boosts the poloidal flow (Figure 3f). Likewise, our model indicates that the slab enters the lower mantle only in the easternmost side, when the Banda slab becomes isolated from the rest of the Indo-Australian slab, and ponds at the base of the upper mantle elsewhere (Figure S9 in Supporting Information S1). This is at odds with most seismic tomography models that indicate that the slab has penetrated the lower mantle all along its strike, indicating that our model dynamics are late with respect to actual penetration of the slab in the lower mantle.

This model reveals the links between complex surface tectonics (slab rollback, trench rotation by more than 90° and encroachment in the Banda embayment) and a simple pattern of mantle flow, only composed of a counterclockwise toroidal flow cell and a poloidal cell. This behavior is captured by the power spectrum of the strain rate (Figures 3i–3l). During early simulation stages, the spectrum is roughly depth-independent, the low frequencies being present at all depths mirroring the concordance between surface flow and surface tectonics, in a quasi-steady state (Figure 3i). After the collision in Papua and subsequent slab breakoff, high frequencies are excited near the surface, but gradually vanish with depth (Figure 3j). That depth dependence of the power spectrum remains from that stage onward, and is further reinforced once the subduction wraps around the Banda embayment and the slab detaches underneath Timor-Wetar (Figures 3k and 3l). This temporal evolution of the power spectrum is conditioned by the structure of the mantle; in the early stages, the Tethyan subduction dominates the poloidal flow; complexity complexity arises once smaller-size structures appear. Overall during transient subduction dynamics, the deep pattern of deformation remains restricted to long-wavelengths, irrespective of the high degree of tectonic complexity that arises in the shallowest layers. The short wavelengths of tectonic activity instead originate from the disruption of the complex structure of the uppermost layers. Prior to the collision of the Australian continent, the surface lithosphere was heterogeneously structured: continental Sundaland in the West and the complex assemblage of continental and oceanic units of Wallacea in the East. The power spectrum during and after the collision of Australia indicates that this small-scale tessellation does not prevent the long-wavelength pattern of surface deformation to resemble that of the underlying mantle flow, but instead superimposes shorter wavelengths that are the cause of the observed short-lived and fast morphotectonic activity that dominate the region.

3.2. Back-Arc Thrust Propagates and Builds Up Toward Subduction Reversal

Intense tectonic activity in and around the subduction arc is another fundamental expression of regional geodynamics. Mega-earthquakes occur on the subduction megathrust as in other subduction zones, but the seismotectonic activity of the back-arc domain, underscored by large magnitude earthquakes like the 1992 M_w 7.8 Flores and 2004 M_w 7.5 Alor earthquakes, is more unusual. The epicenters of these destructive earthquakes punctuate the Flores and Wetar back-arc thrusts that developed during the Australian continent impingement into the subduction zone (Figure 1) (Koulali et al., 2016; Silver et al., 1983). The 2018 M_w 6.9 Lombok earthquake sequence highlighted the westward propagation of the thrust from the Flores and Wetar back-arc thrusts. The Lombok events occurred on blind thrusts (Yang et al., 2020), indicative of an early stage of faulting, which invigorates the question of the propagation of the fault into continental Sundaland. Mounting tectonic and geodetic evidence suggest that the Baribis and Kendeng thrusts of Java island (Figure 1) stem from the Flores and Wetar back-arc thrusts (Koulali et al., 2016) and form a continuous Java back-arc thrust. Are these discontinuous faults merging into a continuous plate scale, an even more forceful thrust that would mark the inception of a subduction reversal?

This scenario is supported by the pattern of surface deformation in our simulation (Figure 4). Strain rates peak in the arc until collision occurs in Papua (Figures 4a and 4b), after which contraction initiates in the back-arc, approximately in the Wetar Flores thrusts (Figures 4c and 4d) and eventually gently propagates westward to enter continental Sundaland at a stage that best compares to the present (Figures 4e and 4f). On the eastern side, the modeled tectonic activity reproduces the severe deformation of the Flores and Wetar back-arc thrusts, strain rates drop more than tenfold when entering Sundaland (from $\sim 5 \times 10^{-15}$ s^{-1} to $\sim 5 \times 10^{-16}$ s^{-1}, Figure 4e). At present, observed and modeled surface deformation fields (Figure 5) are in good agreement. Model velocities after the collision of the Australian continent decrease to rates that are approximately twice smaller than current geodetic rates (see also Figure S1 in Supporting Information S1), but show a remarkably consistent pattern of deformation. Both geodetic and modeled velocities strongly decrease westward along the island arc (with respect to stable Sundaland) with a reduction in the northward velocity at the edge of continental Sundaland. This result is further

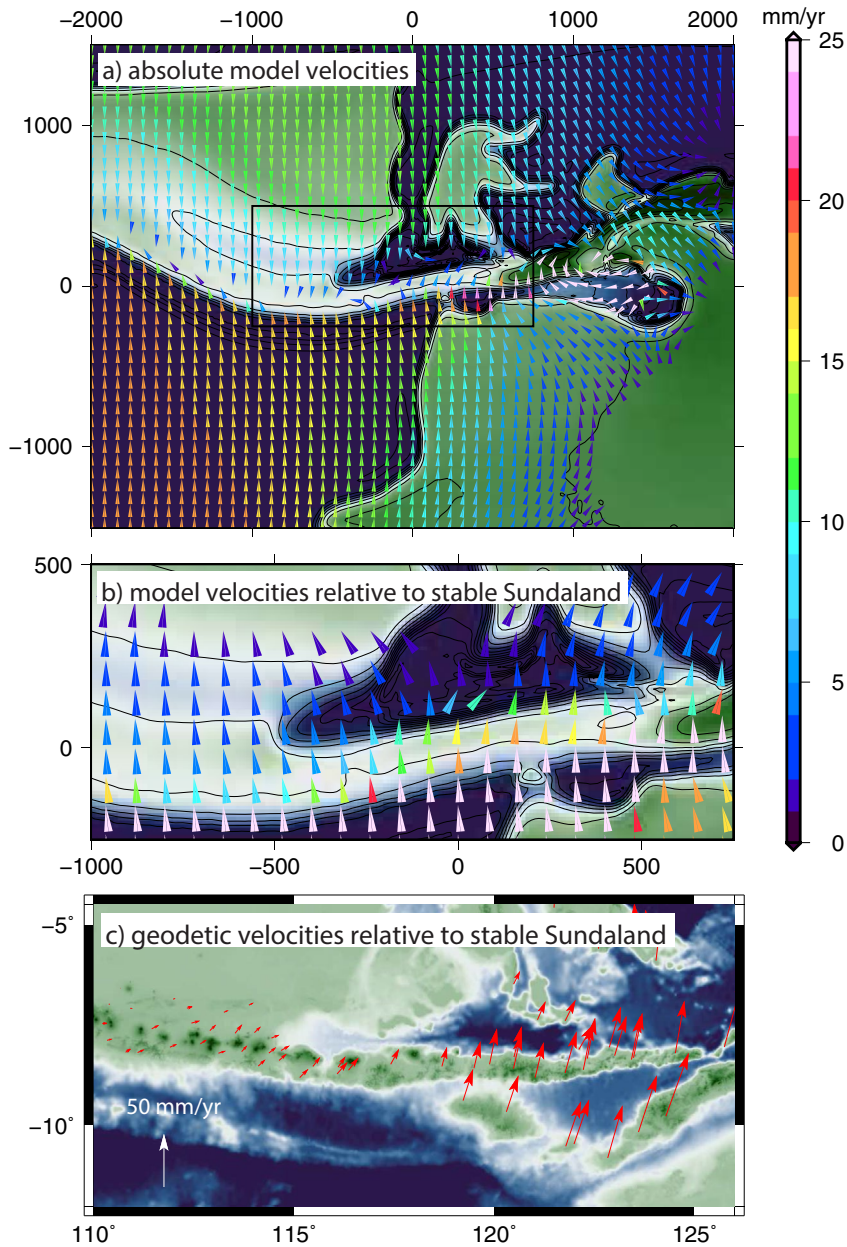

Figure 5. Observed and modeled surface velocities. (a) Global velocities in the model reference frame; (b) zoomed in velocities, with respect to stable Sundaland (at coordinate −500/500 km). (c) Geodetic velocities relative to Sundaland (Koulali et al., 2016) at an approximately comparable geographical scale than in panel (b).

reinforced by the similarity between strain rates (Figure 4e) and geodetically derived strain rates (Figure S10 in Supporting Information S1).

Structural observations, indicative of the bulk deformation, are also compatible: while shortening in the eastern part of the arc (including Sumba, Flores, and Timor islands) is characterized by important nappe stacking, back-arc thrusting and fast uplift, Java island at the southern rim of Sundaland is affected by the modest Plio-Quaternary fold and thrust belt in the Kendeng hills of East Java, and the even more modest thrusts of the Baribis fault zone in the West (Clements et al., 2009; Simandjuntak & Barber, 1996). The model outcome, when compared to these tectonic and kinematic observations, suggests that the Wetar-Flores back-arc thrusts are currently merging and prograding westward, entering Java island where the Java back-arc thrust would be the active propagator of the fault. As it is common practice in atmospheric science, numerical models permit to be predictive by

deduction. Here, predictions for future times from our simulations (Figures 4g and 4h) suggest that the deformation in the back-arc will eventually evolve into a major and continuous south verging thrust that will ultimately become the most active structure of the region. During the process, subduction will initiate after small oceanic basins in Wallacea begin to subduct along that fault, leading to subduction polarity reversal. These small oceanic basins, which spread southward during Banda slab rollback, will disappear while the subduction reverses, with a northward-retreating trench.

3.3. Dynamic Topography Drowns Down the Weber Basin to 7,000 m

Banda subduction dynamics quickly evolved throughout the course of the Australian convergence. In particular, as the trench hides away in the Banda embayment, its curvature increases, and it now tightly confines the Weber and Banda basins. As a young oceanic basin (~3 Ma or less; Hinschberger et al., 2005), the Weber basin is expected to stand at shallower depths. Likewise, the adjacent North and South Banda Basin, which opened earlier during the Miocene, lie at considerable depths (4,000–5,000 m). The anomalous depth of the Weber Deep has been tentatively linked to tectonics (Pownall et al., 2016), but it is unclear how even an overly thinned lithosphere would reach much greater depths than that of back-arc basins or oceanic ridges, for instance. If the comparison with ridges holds, the residual topography (i.e., the component of the topography that departs from isostatic equilibrium) of such a young basin is undoubtedly in excess of several kilometers, for which explanations are lacking.

During the retreat and curvature of subduction trenches, the convexity of slabs also increases as they sweep into the mantle (Loiselet et al., 2009). The mass anomalies of dense slabs get concurrently more and more focused underneath their back-arc basins, similarly to mantle downwellings that accompany slab descent. The vertical traction exerted by the viscous flow underneath the Earth's surface accordingly increases and warps the surface downward above the mass anomaly (Husson, 2006). As the slab breaks off, the mass excess gets deeper, vertical tractions at the surface decrease, and the topography returns to isostatic equilibrium. This scenario applies very well to the Weber and Banda basins for which our model permits the evaluation of the magnitude of this dynamic topography (Figure 6). As the slab enters the Banda embayment (25.5 My model time), it gets tightly squeezed between the northern arc (equivalent to Seram) and the northward migrating Australian margin; the predicted dynamic deflection reaches its maximal value (Figures 6b and 6c). Retreat proceeds and dynamic topography decreases because the slab flattens as it lies at the bottom of the upper mantle, and because the slab tears to the North of Australia. The situation that most resembles the present in the model (when the trench meets the eastern end of the Banda embayment) is slightly delayed with respect to the reference stage that regionally matches the geodynamic evolution (by ~1.8 My, 28.7 My instead of 26.9 My, see above). At that stage, the predicted dynamic deflection above the subduction (from the trench to the Western part of the basin) warps down the basin from ~4 km in the West to ~7 km in the East (Figure 6c). Our model suggests that this ~3 km deep deflection could have been even larger during the earlier stages (25.5 and 26.9 My, Figure 6c) when the dynamic deflection of the topography peaked to ~4 km and drowned the basin to ~8 km before declining. As the slab breaks off, the amplitude decreases and topography will be almost back to isostasy at 31.2 My (model time).

These simulations suggest that the Weber Deep and more generally the Banda basin largely owe their exceptional depths to dynamic topography. This deflection is likely the most important one on Earth. Other back-arc basins lie at considerable depths in similar settings, but none is as deep as the Weber Deep. In continental domains, the basement below the Focsani (Carpathians) and Ganga (Himalaya) foreland basins is subsided down to 13 and 8 km depths by dynamic subsidence (Husson et al., 2014; Şengül-Uluocak et al., 2019), but they only surpass the Weber Deep because the sediment load reinforces the deflections. Our model results also indicate that the Banda arc and affiliated basins are currently uplifting as dynamic topography decreases. This result partly explains the ubiquitous uplifted Pleistocene coral reef sequences that festoon the islands of the Banda arc (Figure 1). Although some are uplifted due to tectonic contraction (for instance, Sumba island, Authemayou et al., 2018, Miller et al., 2021, or SE Sulawesi, Pedoja et al., 2018), the background uplift of the region is induced by the relaxation of the dynamic topography. This motion is well localized around the basin, while the Australian margin conversely continues to subside at present.

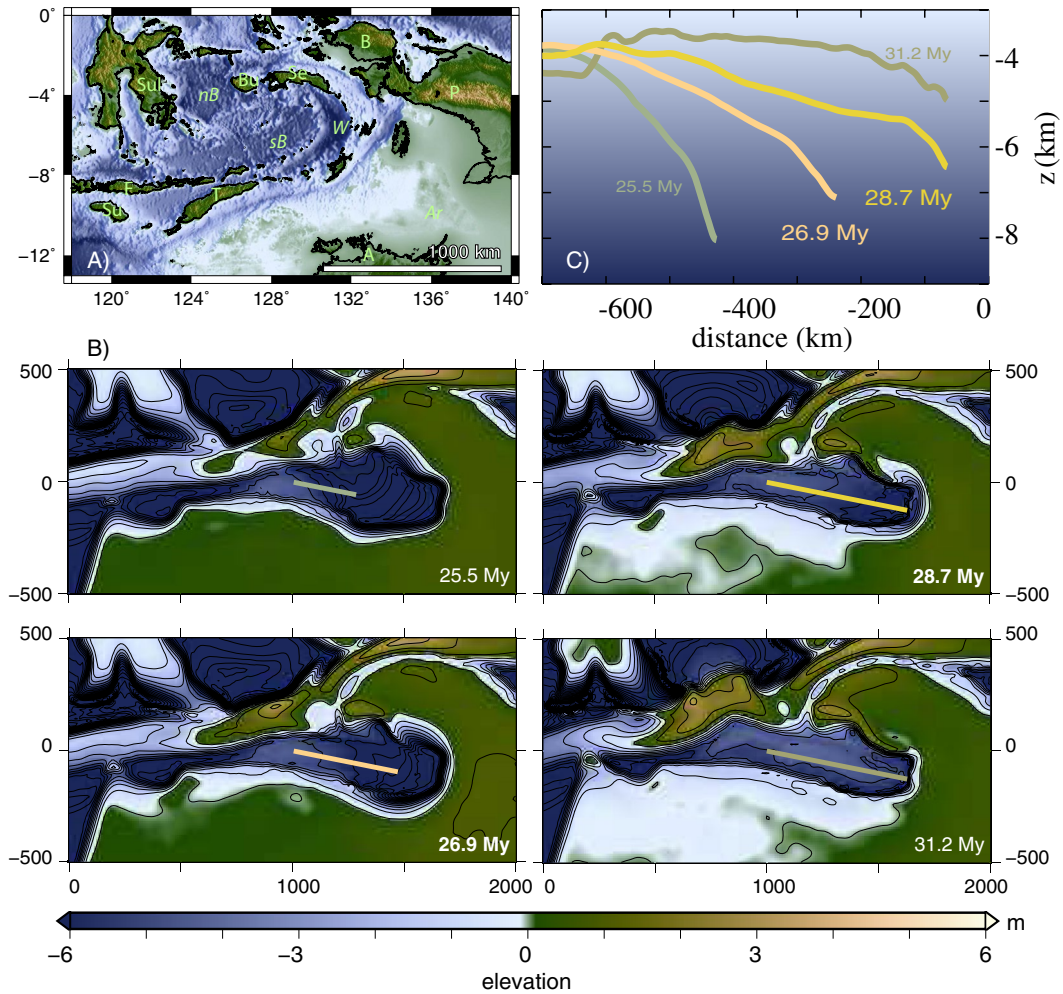

Figure 6. Dynamic topography in the Banda arc and Weber Deep. (a) Bathymetry, Sul, Sulawesi; Bu, Buru; Se, Seram; B, Bird's Head; P, Papua; A, Australia; T, Timor; F, Flores; Su, Sumba; Ar, Arafura sea; nB, sB, North and South Banda basins; W, Weber Deep. (b) Modeled topography during Banda arc formation, (c) Profiles of predicted dynamic topography (water-compensated—Section 2), truncated in the East at the location of the subduction trench to show the upper plate only. Location Figure 3f.

3.4. Dynamic Subsidence in the Sunda and Sahul Shelves

The Banda basin and neighboring islands broadly define the mostly uplifting region of Wallacea, while at its South and West, it is surrounded by the flooded continental platforms of Sahul and Sundaland (Figure 1). They stand above a "subduction graveyard," where considerable amounts of oceanic lithosphere have been drawn down in the mantle within multiple subduction zones. These flooded continents have long been assigned to the dynamic topography associated with whole-mantle circulation at present-day (Conrad & Husson, 2009; Gurnis, 1993; Ricard et al., 1993). The vertical traction exerted by the downwelling mantle warps the surface of the Earth downward enough to expose continents to marine transgressions. More specifically, subsidence in Sahul is thought to have increased over time as the continent approaches the subduction and overrides the Indo-Australian subducting plate (DiCaprio et al., 2011); long term subsidence of Sundaland is proposed to result from slab avalanching in the lower mantle (T. Yang et al., 2016). At present-day, both continental platforms subside at a few tens of mm/yr (Figure 1), about 10 times faster than the slow subsidence predicted from subduction dynamics models (DiCaprio et al., 2011; T. Yang et al., 2016). In addition, hectic movements of uplift and subsidence are reported in Sahul since Late Miocene (Gurnis et al., 2020).

The topography of North Australia, the "tilting continent" (Sandiford, 2007) dips toward the trench (Figure 7a) by ∼0.4‰ on average. Our models predict extremely comparable values of dynamic tilt (Figure 7b). In addition,

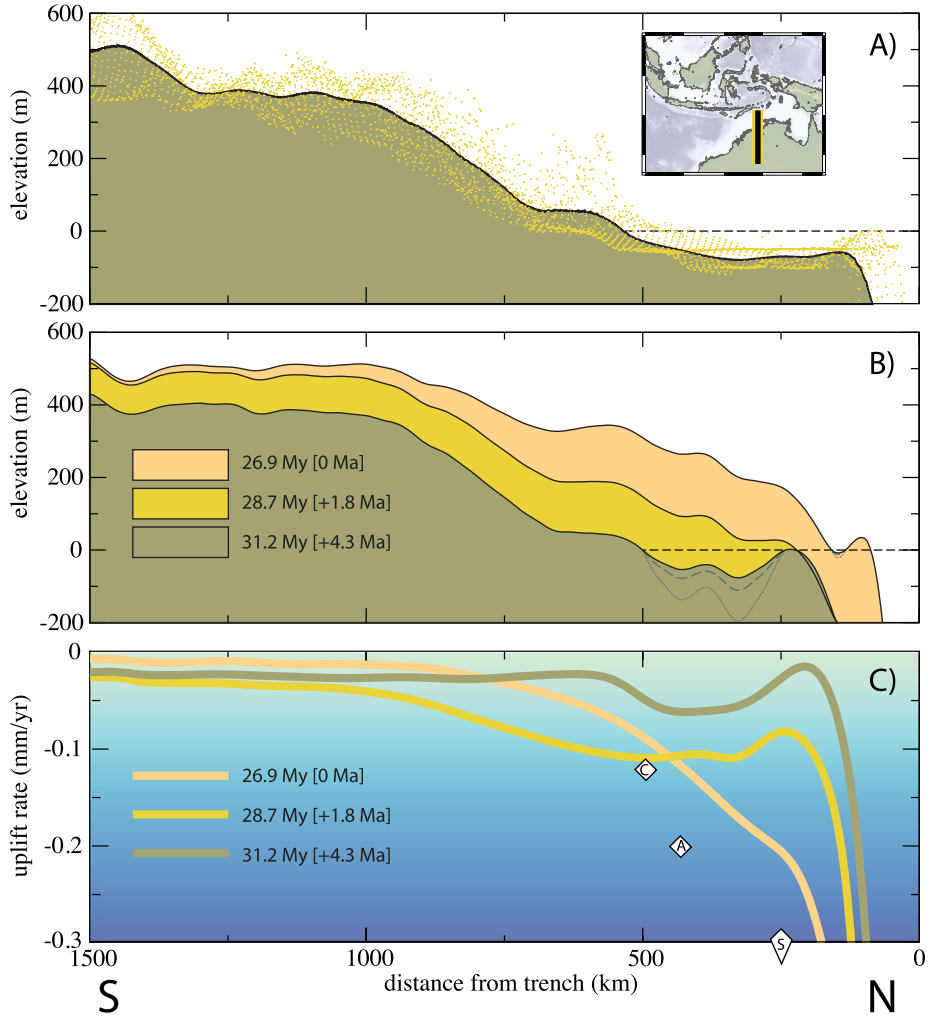

Figure 7. Australia, "the tilting continent" (Sandiford, 2007). (a) Swath topographic profile across the northern half of Australia (solid curve: average, location in inset map). (b) Predicted topography (water-compensated—gray dashed line—and sediment-compensated—gray dotted line—platform bathymetries are shown for completeness). (c) Uplift rates at three model time steps. Diamonds show observations of Late Pleistocene subsidence rates (S, Scott reef; A, Adele reef; C, Cockatoo Island, see Supporting Information S1).

the topographic profiles are very similar, showing maximal slopes between 500 and 1,000 km from the trench (Figures 7a and 7b, particularly after 31.2 My model time; again, slightly delayed with respect to the regional "reference stage" at 26.9 My). Subsidence rates also vary over time, and at present-day, they only slightly exceed estimates of Pleistocene subsidence based on observations (Figure 7c). Our simulation confirms that the northward tilt of Australia is caused by the dynamic deflection of the descending slab. Revived subsidence at present-day happens in our simulation during slab tearing. The toroidal flow strengthens from this slab hole (online animation S2) which facilitates the descent of the slab and its retreat underneath NE Australia, relocating dynamic subsidence from the Banda basin toward Australia. This process makes subsidence rates quickly vary in time, but also spatially in North Australia (Figure 8). This quickly evolving pattern in turn explains the fast and "reversible subsidence" observed in the NE margin of Australia (Gurnis et al., 2020).

The Sunda shelf, in the North of the Indonesian arc, lies at shallower depths than 100 m. Seismic reflection (Figure 9a) reveals that the flat continental platform is tilted southward by ~0.6% and that sedimentary layers level the surface. Our model predicts comparable tilting due to dynamic topography (Figure 9b), which permits to assign a dynamic origin to the tilt of Sundaland. The amplitude of the deflection is larger than that of Sahul because the Sunda shelf lies on the upper plate and is therefore located above the dense, northward dipping subducting mass anomaly of the slab. The sedimentary infill is unconformably disposed and shows a northward progradation of

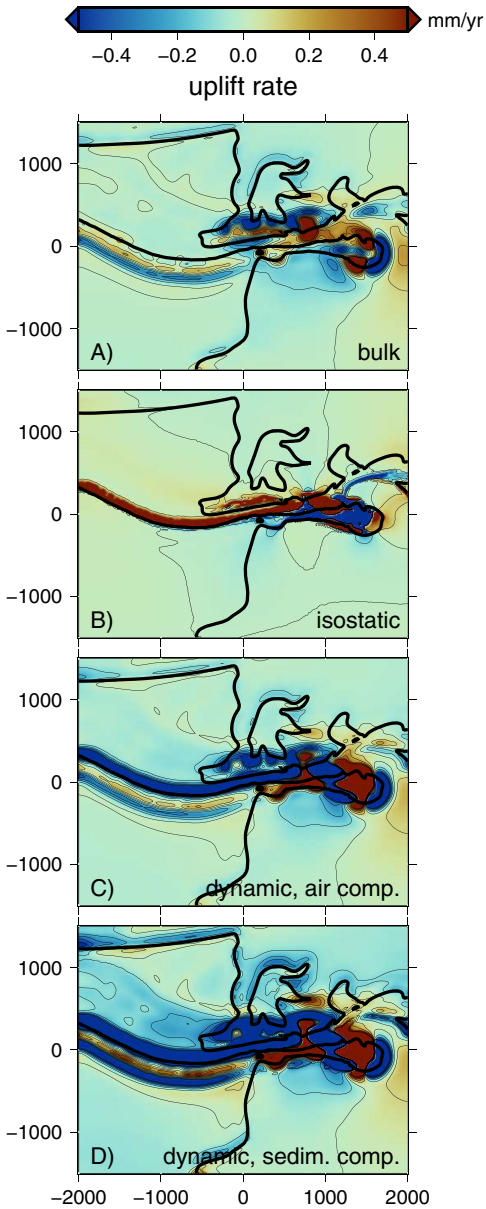

Figure 8. Modeled uplift rates after 26.9 My (model time). (a) Bulk, (b) isostatic, (c) dynamic, assuming air-loading, and (d) dynamic, assuming sediment-loading (see Section 2).

onlapping sediments; the sedimentary layers are thickening southward in a fan shape. While the unconformity indicates that the tilt precedes to a large extent the deposition of the sediments since Miocene (Smyth et al., 2008), the deposition pattern is that of a broad trenchward-increasing subsiding basin. At present-day, subsidence rates amount to 0.1–0.3 mm/yr (Figure 1). Our simulation shows that most of the deflection was acquired during early stages of subduction (Figure 4d), but that subsidence resumed after the northern margin of Australia collided with the arc (Figure 4e), yielding subsidence rates in the range of the geological estimates (Figures 7c, 9b, and 9c). During these events, dynamic subsidence rates in Sundaland varied through time: during the initial stages of oceanic subduction, poloidal flow over the large Indo-Australian subducting plate deflected the upper plate. Following the collision of Australia, both slab detachment underneath Papua and slab tearing underneath Timor fostered the development of a toroidal cell over a now narrower Indian oceanic slab (Figures 3d–3f). Subduction and mantle flow rates increased, reinforcing the dynamic warping of the upper plate originally acquired during pre-collisional stages, thereby causing the subsidence that currently prevails.

4. Discussion

The setup of our model was designed to resemble Early to Mid-Miocene reconstructions at the starting stage, in a need to facilitate a close match to an extensive set of morphotectonic observations. One of the main outcomes of this simulation is to reveal how surface complexity can be induced by a much simpler mantle circulation scheme at depth. While the Banda-Java subduction zone displays an apparent tumult of various morphotectonic expressions at the surface, the underlying mantle flow is the mere adjunction of a counterclockwise toroidal cell (starting when the slab initially detached underneath Papua) to the dominantly poloidal flow that exists as long as subduction proceeds. The slowly evolving pattern of mantle flow in the aftermath of the collision of the Australian continent with Papua and with the Banda arc remains simply structured. It nevertheless remodels the physiography at various scales: jerks of dynamic subsidence are excited by slower subduction dynamics. If morphotectonic time and space scales do not seem to match between the surface and the mantle, it is because mantle flow enters a transient phase that relocates stresses underneath the already structured surface lithosphere. Surface tectonics indicate that horizontal stresses quickly vary, and subsidence rates reveal that changes in dynamic topography can be very fast. The "surface expression of mantle convection" may also occurs at faster rates and shorter space scales than the very mechanism it originates from (Figure 3, Coltice et al., 2019; Mallard et al., 2016). While the long-wavelength pattern of deformation adjusts to that of the underlying mantle flow, the short-wavelength deformation is the transient response of the tessellated, heterogeneous lithosphere. Such relationships are likely valid at other plate boundaries that the SE Asian region illustrates more than elsewhere.

From a regional standpoint, our model mechanically validates the earlier conceptual scenario proposing that the Indo-Australian subducting slab rolled back and curled up around Papua before molding the Banda embayment (Milsom, 2001; Spakman & Hall, 2010). However, in our simulation, the fate of the Banda slab differs. It is inexorably torn and eventually detached underneath Timor-Wetar before it reaches the far East Banda arc. Although seismic models are inconsistent regarding the existence of a slab window in this region (Ely & Sandiford, 2010; Hall & Spakman, 2015; Harris et al., 2020; Porritt et al., 2016; Widiyantoro & van der Hilst, 1997; Widiyantoro et al., 2011; Zenonos et al., 2019), this result is difficult to reconcile with the most recent seismic studies that state that slab integrity is preserved. If the rollback model holds, geometrical consistency (or, put differently, mass

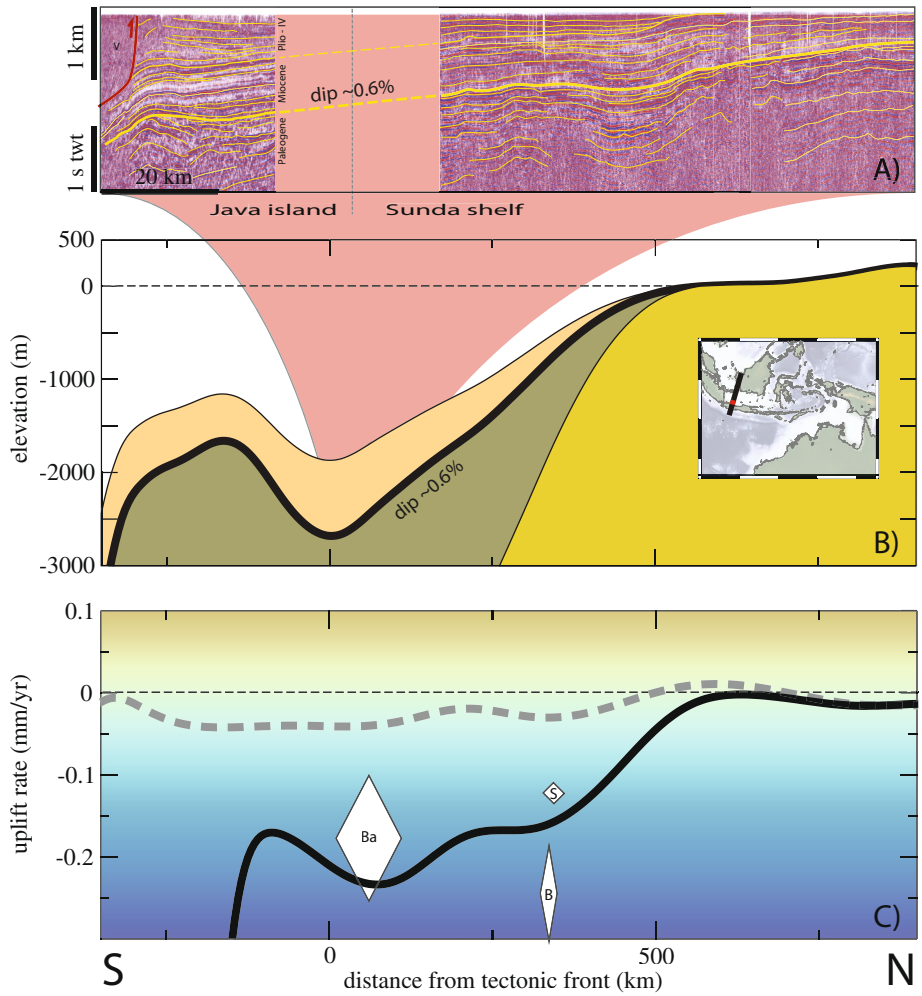

Figure 9. "Subsiding Sundaland" (Sarr, Husson, et al., 2019). (a) Seismic profile across the Sunda shelf (courtesy Pusdatin ESDM Indonesia, location as a red bar in inset map; conversion from two-way times to meters assuming a uniform wave speed of 1,800 m/s in sediments); V, Volcanic rocks (undated, but still active). (b) Predicted topography (model-equivalent location in inset map), for three surface loading hypotheses: air-compensated (orange), water-compensated (green), sediment-compensated (yellow). Scales are different for panels (a and b). (c) Predicted uplift rates. Bulk (gray dashed line) and dynamic subsidence (solid curve, see Methods). Diamonds show observations of Late Pleistocene subsidence rates (B, Belitung; Ba, Bawean; S, Singapore, see Section 2).

conservation) invites reappraising seismic tomography models. One limitation of the model could conversely be turned into a means to lift the paradox between the dynamic and seismological standpoints: while we used state-of-the art rheologies in our models, we acknowledge that the mechanical behavior is only known to a certain extent. Less viscous oceanic lithospheres or a more dynamic rheology at continental margins could possibly hold the Banda slab longer while allowing for its efficient stretching without tearing. Likewise, decoupling of the mantle lithosphere from the crust could facilitate the subduction of the mantle lithosphere (Capitanio et al., 2010). However, given the current knowledge, such fine-tuning of the models would be fraught with unsupported speculations. Conversely, the successful and scrupulous model predictions of several morphotectonic features that we deem diagnostic of the processes at play come in support of the dynamic scenario. The excellent agreement between observations and models indicates that, following slab rollback in the Banda embayment, subsequent rerouting of mantle flow during slab detachment underneath Timor-Wetar subsided the Weber basin to abyssal depths and reinvigorated warping and flooding in the Sundaland and Sahul continental platforms until present. Concurrently, compression increases in the arc, causing the Wetar-Flores back-arc thrust to quickly propagate westward into continental Sundaland while subduction polarity is on the brink to reverse. Other data, such as the

nature of the volcanism or a comprehensive analysis of seismic anisotropy could help settle the long-lived debate regarding existence of a detached slab underneath eastern Indonesia.

A natural follow-up of this study would be to address the interaction of the solid Earth with the soft Earth. The quickly evolving Late Cenozoic physiography of Southeast Asia interacts with the hydro-, atmo-, and bio-spheres of the Earth likely more dynamically than anywhere else (Molnar & Cronin, 2015; Salles et al., 2021; Sarr, Sepulchre, & Husson, 2019). High-resolution geodynamic models like the current one permit to envision a consistent integration of all Earth's spheres at once.

5. Conclusion

At the eastern end of the Tethys, the subduction of the Indo-Australian plate underneath Southeast Asia ideally permits to investigate the expression of a single, long-wavelength geodynamic event on the morphotectonic activity at various time and space scales. The current "Earth-like" numerical simulation of the subduction zone shows that: (a) Docking of the Australian continent onto the subduction arc disrupted the mostly cylindrical mantle flow by adding a long-wavelength toroidal flow cell to the existing long-wavelength poloidal flow cell. (b) Mantle coupling to the previously structured lithosphere causes many short-lived and small-scale tectonic perturbations, as exemplified by slab rollback and curling into the Banda embayment, back-arc thrusting and future subduction reversal to the North of Timor-Wetar, or lateral propagation of the back-arc thrust onto Java island. (c) The Weber superdeep basin owes its exceptional bathymetry to the concentration of mass anomalies related to the subducting slab around the Banda arc. This is the largest amplitude of dynamic topography on Earth. (d) Dynamic subsidence in the North of Australia increases as it gets closer and overrides its own oceanic slab. (e) Dynamic topography over the Indian slab floods the Sunda shelf. The revised subduction dynamics following the collision of the Australian continent fosters dynamic subsidence at present-day. The magnitudes, rates, and velocities of all these morphotectonic events are not only high, compared to other subduction zones, but are also caused by a unique geodynamic event.

Data Availability Statement

Seismic data were obtained courtesy of Pusdatin ESDM, Indonesia (MoU LIPI, Indonesia). Numerical code LaMEM (*9*) is available at https://bitbucket.org/bkaus/lamem. All maps were done with GMT (Wessel et al., 2019). All other data needed to evaluate the conclusions in the paper are present in the paper and/or the Supplementary Materials.

Acknowledgments
This research was partially funded by National Geographic Society, Lembaga Pengelola Dana Pendidikan, Nusantara Hubert Curien partnership, and European Research Council. The authors are grateful to O. H. Göğüş and to our editors for their constructive reviews. No other unpublished data were used or created for this research.

References

Authemayou, C., Brocard, G., Delcaillau, B., Molliex, S., Pedoja, K., Husson, L., et al. (2018). Unraveling the roles of asymmetric uplift, normal faulting and groundwater flow to drainage rearrangement in an emerging karstic landscape. *Earth Surface Processes and Landforms*, *43*, 1885–1898. https://doi.org/10.1002/esp.4363

Capitanio, F. A., Morra, G., Goes, S., Weinberg, R., & Moresi, L. (2010). India-Asia convergence driven by the subduction of the Greater Indian continent. *Nature Geoscience*, *3*, 136–139. https://doi.org/10.1038/ngeo725

Clements, B., Hall, R., Smyth, H. R., & Cottam, M. A. (2009). Thrusting of a volcanic arc: A new structural model for Java. *Petroleum Geoscience*, *15*, 159–174. https://doi.org/10.1144/1354-079309-831

Coltice, N., Husson, L., Faccenna, C., & Arnould, M. (2019). What drives tectonic plates? *Science Advances*, *5*, eaax4295. https://doi.org/10.1126/sciadv.aax4295

Conrad, C. P., & Husson, L. (2009). Influence of dynamic topography on sea level and its rate of change. *Lithosphere*, *1*, 110–120. https://doi.org/10.1130/l32.1

Das, S. (2004). Seismicity gaps and the shape of the seismic zone in the Banda Sea region from relocated hypocentres. *Journal of Geophysical Research*, *109*, B12303. https://doi.org/10.1029/2004jb003192

Davies, D. R., Valentine, A. P., Kramer, S. C., Rawlinson, N., Hoggard, M. J., Eakin, C. M., & Wilson, C. R. (2019). Earth's multi-scale topographic response to global mantle flow. *Nature Geoscience*, *12*, 845–850. https://doi.org/10.1038/s41561-019-0441-4

DiCaprio, L., Gurnis, M., Müller, R. D., & Tan, E. (2011). Mantle dynamics of continentwide Cenozoic subsidence and tilting of Australia. *Lithosphere*, *3*, 311–316. https://doi.org/10.1130/l140.1

Ely, K. S., & Sandiford, M. (2010). Seismic response to slab rupture and variation in lithospheric structure beneath the Savu Sea, Indonesia. *Tectonophysics*, *483*, 112–124. https://doi.org/10.1016/j.tecto.2009.08.027

Gurnis, M. (1993). Phanerozoic marine inundation of continents driven by dynamic topography above subducting slabs. *Nature*, *364*, 589–593. https://doi.org/10.1038/364589a0

Gurnis, M., Kominz, M., & Gallagher, S. J. (2020). Reversible subsidence on the North West Shelf of Australia. *Earth and Planetary Science Letters*, *534*, 116070. https://doi.org/10.1016/j.epsl.2020.116070

Hall, R. (2012). Late Jurassic-Cenozoic reconstructions of the Indonesian region and the Indian Ocean. *Tectonophysics*, *570–571*, 1–41. https://doi.org/10.1016/j.tecto.2012.04.021

Hall, R. (2017). Southeast Asia: New views of the geology of the Malay Archipelago. *Annual Review of Earth and Planetary Sciences*, *45*, 331–358. https://doi.org/10.1146/annurev-earth-063016-020633

Hall, R., & Spakman, W. (2015). Mantle structure and tectonic history of SE Asia. *Tectonophysics*, *658*, 14–45. https://doi.org/10.1016/j.tecto.2015.07.003

Harris, C. W., Miller, M. S., Supendi, P., & Widiyantoro, S. (2020). Subducted lithospheric boundary tomographically imaged beneath arc-continent collision in eastern Indonesia. *Journal of Geophysical Research: Solid Earth*, *125*. https://doi.org/10.1029/2019JB018854

Harris, R. (2011). The nature of the Banda Arc–continent collision in the Timor region. In D. Brown & P. D. Ryan (Eds.), *Arc continent collision*. *Frontiers in Earth Sciences* (pp. 163–211). Springer Berlin Heidelberg. https://doi.org/10.1007/978-3-540-88558-0_7

Hinschberger, F., Malod, J.-A., Réhault, J. P., Villeneuve, M., Royer, J. Y., & Burhanuddin, S. (2005). Late Cenozoic geodynamic evolution of eastern Indonesia. *Tectonophysics*, *404*, 91–118. https://doi.org/10.1016/j.tecto.2005.05.005

Hirth, G., & Kohlstedt, D. (2004). Rheology of the upper mantle and the mantle wedge: A view from the experimentalists. In J. Eiler (Ed.), *Inside the subduction factory* (Vol. 138, pp. 83–106). American Geophysical Union. https://doi.org/10.1029/138GM06

Holmes, A. (1931). Radioactivity and Earth movements. *Nature*, *128*, 419. https://doi.org/10.1038/128496e0

Husson, L. (2006). Dynamic topography above retreating subduction zones. *Geology*, *34*, 741–744. https://doi.org/10.1130/g22436.1

Husson, L., Bernet, M., Guillot, S., Huyghe, P., Mugnier, J. L., Replumaz, A., et al. (2014). Dynamic ups and downs of the Himalaya. *Geology*, *42*, 839–842. https://doi.org/10.1130/g36049.1

Husson, L., Boucher, F. C., Sarr, A. C., Sepulchre, P., & Cahyarini, S. Y. (2019). Evidence of Sundaland's subsidence requires revisiting its biogeography. *Journal of Biogeography*, *47*, 843–853. https://doi.org/10.1111/jbi.13762

Jolivet, L., Faccenna, C., Becker, T., Tesauro, M., Sternai, P., & Bouilhol, P. (2018). Mantle flow and deforming continents: From India-Asia convergence to Pacific subduction. *Tectonics*, *37*, 2887–2914. https://doi.org/10.1029/2018tc005036

Kaus, B. J. P., Popov, A. A., Baumann, T. S., Pusok, A. E., Bauville, A., Fernandez, N., & Collignon, M. (2016). Forward and inverse modelling of lithospheric deformation on geological timescales. *Proceedings of NIC Symposium* (Vol. 48, pp. 978–983).

Koulali, A., Susilo, S., McClusky, S., Meilano, I., Cummins, P., Tregoning, P., et al. (2016). Crustal strain partitioning and the associated earthquake hazard in the eastern Sunda-Banda Arc. *Geophysical Research Letters*, *43*, 1943–1949. https://doi.org/10.1002/2016gl067941

Loiselet, C., Husson, L., & Braun, J. (2009). From longitudinal slab curvature to slab rheology. *Geology*, *37*, 747–750. https://doi.org/10.1130/g30052a.1

Mackwell, S. J., Zimmerman, M. E., & Kohlstedt, D. L. (1998). High-temperature deformation of dry diabase with application to tectonics on Venus. *Journal of Geophysical Research*, *103*(B1), 975–984. https://doi.org/10.1029/97JB02671

Mallard, C., Coltice, M., Seton, M., Müller, R. D., & Tackley, P. J. (2016). Subduction controls the distribution and fragmentation of Earth's tectonic plates. *Nature*, *535*, 140–143. https://doi.org/10.1038/nature17992

Miller, M. S., Zhang, P., Dahlquist, M. P., West, A. J., Becker, T. W., & Harris, C. W. (2021). Inherited lithospheric structures control arc-continent collisional heterogeneity. *Geology*, *49*, 652–656.

Milsom, J. (2001). Subduction in eastern Indonesia: How many slabs? *Tectonophysics*, *338*, 167–178. https://doi.org/10.1016/s0040-1951(01)00137-8

Molnar, P., & Cronin, T. W. (2015). Growth of the maritime continent and its possible contribution to recurring ice ages. *Paleoceanography*, *30*, 196–225. https://doi.org/10.1002/2014pa002752

Pedoja, K., Husson, L., Bezos, A., Pastier, A. M., Imran, A. M., Arias-Ruiz, C., et al. (2018). On the long-lasting sequences of coral reef terraces from SE Sulawesi (Indonesia): Distribution, formation, and global significance. *Quaternary Science Reviews*, *188*, 37–57. https://doi.org/10.1016/j.quascirev.2018.03.033

Porritt, R. W., Miller, M. S., O'Driscoll, L. J., Harris, C. W., Roosmawati, N., & Teofilo da Costa, L. (2016). Continent–arc collision in the Banda Arc imaged by ambient noise tomography. *Earth and Planetary Science Letters*, *449*, 246–258. https://doi.org/10.1016/j.epsl.2016.06.011

Pownall, J. M., Hall, R., & Lister, G. S. (2016). Rolling open Earth's deepest forearc basin. *Geology*, *44*, 947–950. https://doi.org/10.1130/g38051.1

Ranalli, G. (1995). *Rheology of the earth* (2nd ed.). Chapman & Hall.

Ricard, Y., Richards, M., Lithgow-Bertelloni, C., & Le Stunff, Y. (1993). A geodynamic model of mantle density heterogeneity. *Journal of Geophysical Research*, *98*, 21895–21909. https://doi.org/10.1029/93jb02216

Royden, L. H., & Husson, L. (2009). Subduction with variations in slab buoyancy: Models and application to the Banda and Apennine systems. In S. Lallemand & F. Funiciello (Eds.), *Subduction zone geodynamics* (pp. 35–45). Springer Berlin, Heidelberg. https://doi.org/10.1007/978-3-540-87974-9_2

Salles, T., Mallard, C., Husson, L., Zahirovic, S., Sarr, A.-C., & Sepulchre, P. (2021). Quaternary landscape dynamics boosted species dispersal across Southeast Asia. *Communications Earth & Environment*, *2*, 240. https://doi.org/10.1038/s43247-021-00311-7

Sandiford, M. (2007). The tilting continent: A new constraint on the dynamic topographic field from Australia. *Earth and Planetary Science Letters*, *261*, 152–163. https://doi.org/10.1016/j.epsl.2007.06.023

Sarr, A. C., Husson, L., Sepulchre, P., Pastier, A.-M., Pedoja, K., Elliot, M., et al. (2019). Subsiding Sundaland. *Geology*, *47*, 119–122. https://doi.org/10.1130/G45629.1

Sarr, A. C., Sepulchre, P., & Husson, L. (2019). Impact of the Sunda Shelf on the climate of the Maritime Continent. *Journal of Geophysical Research: Atmospheres*, *124*, 2574–2588. https://doi.org/10.1029/2018jd029971

Şengül-Uluocak, E., Pysklywec, R. N., Göğüş, O. H., & Ulugergerli, E. U. (2019). Multidimensional geodynamic modeling in the Southeast Carpathians: Upper mantle flow-induced surface topography anomalies. *Geochemistry, Geophysics, Geosystems*, *20*, 3134–3149.

Silver, E. A., Reed, D., McCaffrey, R., & Joyodiwiryo, Y. (1983). Back arc thrusting in the eastern Sunda arc, Indonesia: A consequence of arc-continent collision. *Journal of Geophysical Research*, *88*, 7429–7448. https://doi.org/10.1029/jb088ib09p07429

Simandjuntak, T. O., & Barber, A. J. (1996). Contrasting tectonic styles in the Neogene orogenic belts of Indonesia. *Geological Society, London, Special Publications*, *106*, 185–201. https://doi.org/10.1144/gsl.sp.1996.106.01.12

Smyth, H., Hall, R., Hamilton, J., & Kinny, P. (2008). East Java: Cenozoic basins, volcanoes and ancient basement. In *Proceedings Indonesia Petroleum Association, 30th Annual Convention* (pp. 251–266).

Solihuddin, T., Collins, L. B., Blakeway, D., & O'Leary, M. J. (2015). Holocene coral reef growth and sea level in a macrotidal, high turbidity setting: Cockatoo Island, Kimberley Bioregion, northwest Australia. *Marine Geology*, *359*, 50–60. https://doi.org/10.1016/j.margeo.2014.11.011

Spakman, W., & Hall, R. (2010). Surface deformation and slab–mantle interaction during Banda arc subduction rollback. *Nature Geoscience*, *3*, 562–566. https://doi.org/10.1038/ngeo917

Susilohadi, S., & Soeprapto, T. A. (2015). Plio-Pleistocene seismic stratigraphy of the Java Sea between Bawean Island and East Java. *Marine Geology of Indonesia*, *32*, 5–16.

Turcotte, D., & Schubert, G. (1982). *Geodynamics*. John Wiley and Sons.

Waelbroeck, C., Labeyrie, L., Michel, E., Duplessy, J. C., McManus, J. F., Lambeck, K., et al. (2002). Sea-level and deep water temperature changes derived from benthic foraminifera isotopic records. *Quaternary Science Reviews*, *21*, 295–305. https://doi.org/10.1016/s0277-3791(01)00101-9

Wessel, P., Luis, J. F., Uieda, L., Scharroo, R., Wobbe, F., Smith, W. H. F., & Tian, D. (2019). The generic mapping tools version 6. *Geochemistry, Geophysics, Geosystems*, *20*, 5556–5564. https://doi.org/10.1029/2019gc008515

Widiyantoro, S., Pesicek, J. D., & Thurber, C. H. (2011). Subducting slab structure below the eastern Sunda arc inferred from non-linear seismic tomographic imaging. *Geological Society, London, Special Publications*, *355*, 139–155. https://doi.org/10.1144/sp355.7

Widiyantoro, S., & van der Hilst, R. (1997). Mantle structure beneath Indonesia inferred from high-resolution tomographic imaging. *Geophysical Journal International*, *130*, 167–182. https://doi.org/10.1111/j.1365-246x.1997.tb00996.x

Yang, T., Gurnis, M., & Zahirovic, S. (2016). Mantle-induced subsidence and compression in SE Asia since the early Miocene. *Geophysical Research Letters*, *43*, 1901–1909. https://doi.org/10.1002/2016gl068050

Yang, X., Singh, S. C., & Tripathi, A. (2020). Did the Flores backarc thrust rupture offshore during the 2018 Lombok earthquake sequence in Indonesia? *Geophysical Journal International*, *221*, 758–768. https://doi.org/10.1093/gji/ggaa018

Zenonos, A., De Siena, L., Rawlinson, N., & Rawlinson, N. (2019). P and S wave travel time tomography of the SE Asia-Australia collision zone. *Physics of the Earth and Planetary Interiors*, *293*, 106267. https://doi.org/10.1016/j.pepi.2019.05.010

Reference From the Supporting Information

Kreemer, C., Blewitt, G., & Klein, E. C. (2014). A geodetic plate motion and global strain rate model. *Geochemistry, Geophysics, Geosystems*, *15*, 3849–3889. https://doi.org/10.1002/2014GC005407